



1 Forecasting dam height and stability of dams formed by rock slope 2 failures in Norway

3 Thierry Oppikofer¹, Reginald L. Hermanns^{1,2}, Vegard U. Jakobsen^{2,*}, Martina Böhme¹, Pierrick
4 Nicolet¹, Ivanna Penna¹

5 ¹Geological Survey of Norway, Leiv Eirikssons vei 39, P.O. Box 6315 Torgarden, 7491 Trondheim, Norway

6 ²Norwegian University of Science and Technology, Trondheim, Norway

7 *Now at: Norwegian Public Roads Administration, Steinskjer, Norway

8 Correspondence to: Thierry Oppikofer (thierry.oppikofer@ngu.no)

9 **Abstract.** Based on an inventory of 69 dams formed by rock slope failures in southwestern Norway and published landslide
10 dam inventories from other parts of the World we developed semi-empirical relationships linking the maximum dam height
11 ($H_{D,max}$ in m) to dam volume (V_D in 10^6 m³) and other relevant parameters such as valley width (W_V in m) or dam area (A_D
12 in km²). Power-laws are obtained for $H_{D,max} = f(V_D)$ and $H_{D,max} = f(V_D, W_V)$, while a linear relationship links $H_{D,max}$ to the
13 ratio V_D/A_D . For dams in southwestern Norway, the linear relationship $H_{D,max} = 1.75 \times V_D/A_D$ has least uncertainties and
14 provides best results when comparing predicted dam heights with a validation dataset composed of existing dams in northern
15 Norway and numerically modelled dams for possible rock slope failures. To assess the stability of future dams we use the
16 predicted dam heights in the dimensionless blockage index DBI and relating this index to the probability of dam failure
17 derived from our dataset and other published databases on landslide dams. This study underlines the potential of semi-
18 empirical relationships for assessing dam height and stability that needs to be included in preliminary hazard and risk
19 assessment for unstable rock slopes, because damming of a river is an important secondary effect of landslides due to
20 upstream flooding and possible outburst floods in case of dam failure.

21 1 Introduction

22 Landslides, and more particularly large rockslides and rock avalanches, have formed natural dams in many mountainous
23 regions (Hewitt, 1982; Costa and Schuster, 1988; Korup, 2002; Casagli et al., 2003; Evans et al., 2011; Hermanns et al.,
24 2011a; Weidinger, 2011; Dufresne et al., 2018). Even large dams with several millions m³ in volume may be unstable and
25 breach (Hewitt, 1998; Dai et al., 2005; Plaza et al., 2011). Many historic events of landslide dam failures are reported to
26 have occurred within a few days to years after the landslide event, causing catastrophic outburst floods in the valley
27 downstream of the dam (Groeber, 1916; Hewitt, 1982; Costa and Schuster, 1988; Evans, 2006) and leading to major
28 destruction and loss of live (Evans et al., 2011).

29 The National landslide database of Norway (NVE, 2020) includes at least 181 historical landslides that caused damming of
30 rivers. Most of them were earth and debris slides (153) and only 22 events were rockslides or rock avalanches. Many of
31 those events created only minor damming of rivers without significant consequences. Yet, there were several major events
32 with significant consequences in terms of loss of life or long-lasting landscape changes: the worst natural disaster in
33 Norway's history occurred on 21 September 1345 when the Gaula River was dammed by a massive debris slide that created
34 a 14 km long lake. After only 2–3 days the dam breached leading to a huge outburst flood in the Gaula Valley burying 48
35 farms and killing at least 500 persons (Furseth, 2006). In 1823, a rock avalanche dammed the Frondøla River and formed
36 the Lintuvatnet Lake (NVE, 2020). The lake is still existing today, even though the dam partially breached leading to an



37 outburst flood in the uninhabited valley. On 26 May 1908, a 1.1 million m³ rock avalanche from the mountain Keipen in the
38 Norang Valley formed a more than 20 m high dam (Fig. 1a, b). The impounded lake Lyngstøylvatnet submerged the road
39 and several mountain farms, whose remains are still visible close to the shoreline (Furseth, 2006, Hermanns et al., 2013b).
40 These historic events emphasize the need of addressing the landslide-damming of rivers in landslide risk analyses, including
41 upriver and potential downriver flooding as well as landslide dam stability assessments (Hermanns et al., 2013b). Massive
42 rock slope failures (RSF) may generate tens of meters high dams with long-lasting and potentially catastrophic consequences.
43 The Geological Survey of Norway systematically maps, investigates and analyzes fractured bedrock slopes that might fail
44 catastrophically in the future (Hermanns et al., 2013a). More than 80 unstable rock slopes that during a catastrophic failure
45 will impact and possibly dam rivers have so far been discovered in Norway (NGU, 2020) (Fig. 2b). These high numbers set
46 the necessity for cost-effective tools to assess dam heights and dam stability for preliminary risk analyses.
47 The most common tool to assess landslide damming in prospective landslide hazard and risk assessments are likely numerical
48 simulations of the landslide propagation (Hungr, 2011). Examples of such numerical models are the DAN3D code
49 (McDougall and Hungr, 2004) or the RAMMS software suite (Christen et al., 2012). However, these models require
50 numerous input parameters and extensive calibration in order to obtain reliable results, which precludes their cost-efficient
51 use for characterization of a large number of sites, as is required in regional studies.
52 Here we establish semi-empirical relationships for the rapid assessment of the maximum dam height, comparable to those
53 developed for landslide run-out (e.g. Scheidegger, 1973; Corominas, 1996) or landslide-generated displacement waves
54 (Oppikofer et al., 2019). We use an inventory of dams formed by rock slope failures (RSF dams) in southwestern Norway
55 (Fig. 2a) along with other published databases on landslide dams (Ermini and Casagli, 2003; Hermanns et al., 2011a; Tacconi
56 Stefanelli et al., 2015) to evaluate the dam height as a function of landslide volume, valley width and dam area. This approach
57 addresses the need for a fast assessment of possible dam formation and stability for potential future RSF, as a part of the
58 systematic hazard and risk analysis of unstable rock slopes in Norway (Hermanns et al., 2012; Oppikofer et al., 2016a,
59 2016b).

60 **2 Methodology**

61 **2.1 Inventory and characteristics of landslide dams**

62 Systematic mapping of RSF dams in southwestern Norway (approximately 120 000 km² in surface) was carried out by
63 Jakobsen (2015) using the online orthophoto map service “Norge i bilder” (Norwegian Mapping Authority, 2020b) and its
64 associated web map service (WMS) in a geographical information system (GIS) (Fig. 1b). This aerial photo analysis focused
65 on present-day lakes as an indicator for possible dams, with the aim of identifying lakes that were impounded by RSF. The
66 analysis investigated therefore the immediate downstream surroundings of lakes, looking for deposits, debris and scars of
67 RSF, but also debris from a possible downstream flooding due to a dam breach. It must be noted that dams without remaining
68 lake are therefore not included in present inventory.

69 The detected dams were mapped and registered in a geospatial database, and their geomorphologic characteristics determined
70 based on orthophotos and the national 10-m digital elevation model (DEM) (Norwegian Mapping Authority, 2020a). These
71 dam characteristics include:

- 72 - the type of landslide that formed the dam, chiefly rock avalanches (massive RSF with several hundred thousand to
73 millions of cubic meter in volume and high mobility) and rockslides/rockfalls (RSF with several thousands to hundred
74 thousands of cubic meter in volume, but without high mobility) or other landslide types;
- 75 - the morphologic dam classifications in plan view and in across-valley and along-valley profiles according to Hermanns
76 et al. (2011b) (Fig. 3);



77 - the dam dimensions including valley width W_V , dam width W_D , dam length L_D , dam area A_D , mean dam height $H_{D,mean}$
78 and maximum dam height $H_{D,max}$, dam volume V_D (Fig. 4);
79 - the upstream catchment area A_C and the resulting DBI-value (Ermini and Casagli, 2003);
80 - an assessment of the dam stability, i.e. whether the dam was unstable and has breached or was (partially) eroded, or was
81 stable and is intact or infilled;
82 - an assessment of any glacial influence on the dam, especially the initial landslide run-out onto a glacier.
83 The dimensions of the dams were directly mapped in the GIS for valley width W_V , dam width W_D , dam length L_D , dam area
84 A_D (Fig. 4a), and the upstream catchment area A_C was calculated using a flow accumulation function in GIS based on the
85 10-m DEM. The mean and maximum dam heights $H_{D,mean}$ and $H_{D,max}$ were estimated based on across-valley and along-valley
86 profiles through the dam (Fig. 4b, c). On those profiles, the possible pre-event topography was extrapolated from the
87 surrounding valley morphology, notably the steepness of the valley flanks and the valley width (Fig. 4b). In along-valley
88 profiles the morphology prior to the dam was based on a linear interpolation between the beginning of the impounded lake
89 and the foot of the dam (Fig. 4c).

90 2.2 Creation of semi-empirical relationships

91 We establish semi-empirical relationships by plotting the maximum dam height relative to various dam characteristics and
92 least-square fitting of functions linking the parameters. The different units of the dam characteristics are accounted for using
93 dimensional analysis. The dam volume V_D , dam area A_D and valley width W_V revealed to be the most relevant dam parameters
94 influencing the maximum dam height $H_{D,max}$, whereas no meaningful correlations were found for other dam characteristics.
95 We assess the inherent uncertainties in the obtained relationships by computing the ratio (ρ) between the measured and
96 predicted maximum dam heights. We then fit cumulative frequency distributions of these ratios using lognormal functions
97 to determine the 95th percentile (ρ_{95}). The ratio ρ_{95} yields the upper bound of the 90% prediction interval, meaning that
98 approximately 5% of the measured maximum dam heights exceed the predicted values by a factor of ρ_{95} or more.
99 The dam morphology certainly influences $H_{D,max}$, it is however difficult to predict without detailed modelling studies, which
100 are beyond the scope of regional studies, for which these semi-empirical relationships are intended. Furthermore, detailed
101 modelling studies most often also include detailed numerical run-out modelling. These run-out models generally provide the
102 thickness of deposits and thus the expected maximum dam height, making the semi-empirical relationships superfluous for
103 detailed local studies.

104 2.3 Forecasting dam height and stability



105 The semi-empirical relationships linking $H_{D,max}$ to relevant parameters are used to predict the dam height for future RSF that
106 could dam a river. The dam height $H_{D,max}$ gets added to the elevation of the riverbed to find the possible elevation of the
107 dammed lake. The extent of the impounded lake is obtained by computing the contour line of the lake elevation in the area
108 upstream to the landslide dam.

109 We use the dimensionless blockage index DBI (Ermini and Casagli, 2003) as a proxy to estimate the likelihood of a dam
110 breach. Low DBI-values depict landslide dams that are most likely stable, whereas a high DBI indicates probably unstable
111 dams. We divide the inventory of RSF dams in southwestern Norway and other inventories (Ermini and Casagli, 2003;
112 Hermanns et al., 2011a; Tacconi Stefanelli et al., 2015) into bins of DBI-values containing each 10-12 dams and calculate
113 the proportion of unstable dams for each bin. We then use these proportions to fit a linear function between the lower limit
114 DBI_{lower} below which dams are considered stable, and the upper limit DBI_{upper} above which dams are deemed unstable. In
115 the transition zone between the lower and upper limits, the likelihood of a dam failure p_f increases linearly (Eq. (1)):



$$p_f = \begin{cases} 0 & \Leftrightarrow DBI \leq DBI_{lower} \\ \frac{DBI - DBI_{lower}}{DBI_{upper} - DBI_{lower}} & \Leftrightarrow DBI_{lower} < DBI < DBI_{upper} \\ 1 & \Leftrightarrow DBI \geq DBI_{upper} \end{cases} \quad (1)$$

117 3 Inventory of landslide dams in southwestern Norway

118 A total of 69 landslide dams are mapped in southwestern Norway (Fig. 2a). Thirty-eight dams were formed by rock
119 avalanches, 29 by rockslides/rockfalls and 2 by debris-flows. We discarded those generated by debris-flows from further
120 analyses because the aim of these empirical relationships is to determine the maximum dam height of future RSF.

121 The frequency of rock avalanches in Norway was highest shortly after the last deglaciation, i.e. between 14 000 and 10 000
122 years BP depending on the location (e.g. Böhme et al., 2015; Hermanns et al., 2017). We therefore assume that also most of
123 the RSF dams in southwestern Norway were formed shortly after the retreat of the Scandinavian ice sheet. However, three
124 dams are most likely influenced by glaciers, notably by depositing on decaying glaciers or on dead-ice bodies in the valley.
125 For 10 other dams such a glacial influence is possible. We excluded these 13 dams from further analyses because their
126 dimensions may have been altered by glaciers and are thus not representative for the present-day situation.

127 According to the landform classification by Etzelmüller et al. (2007), most of the 54 remaining dams are in regions with
128 “extreme Alpine relief with over-deepened glacial valleys” or in “high paleic mountain regions with glacial incisions” (Fig.
129 2a). In Rogaland County in southern Norway several clusters of RSF dams are observed in the landform types “glacially
130 scoured low mountains and valleys” and “mountain plateaus” (Fig. 2c). These clusters are closely related to WSW-ENE-
131 trending faults (Gabrielsen et al., 2002) forming escarpments that are prone to RSF. Twenty-one dams are intact with a
132 dammed lake and 10 other dams are filled by sediments except a small residual lake. On the side of unstable dams, 16 dams
133 are classified as eroded because no deposits of an outburst flood are visible, and 7 dams have failed and likely led to an
134 outburst flood as suggested by related deposits downriver.

135 The morphologic dam classification in plan view according to Hermanns et al. (2011b) reveals that most dams are formed
136 by a RSF completely crossing the valley (Type IIa, $n=36$) (Fig. 3a). Partial damming of the valley by a RSF occurred in 5
137 cases (Type IIc), and 5 dams have multiple lakes (Type IIIa). The across-valley profiles can be classified as symmetrical
138 deposits in a symmetrical valley in 24 cases (Type i), and as asymmetrical with thickest deposits in the distal part in 19 cases
139 (Type ii) (Fig. 3b). The classification of the along-valley profiles reveals 21 dams with low thickness and gentle slopes (Type
140 1) due to the absence of constraints in the valley morphology (Hermanns et al., 2011b), and 29 dams with high thickness
141 and steep slope (Type 2) in a confined valley setting (Fig. 3c).

142 Table 1 summarizes the dimensions of the RSF dams in the inventory. The dam length L_D ranges from 45 to 1600 m with a
143 median length of 200 m, whereas the dam width W_D tends to be larger by a factor of 1.7 (median of ratio W_D/L_D) and ranges
144 from 45 to 2800 m with a median width of 330 m. The dam area covers three orders of magnitude with values between
145 5000 m² to 2.7 km² with a median of 53 000 m². The maximum dam heights $H_{D,max}$ vary between 5 and 210 m, whereas the
146 mean dam heights $H_{D,mean}$ vary between 2 and 113 m. The median dam heights are 21 m and 12 m for $H_{D,max}$ and $H_{D,mean}$,
147 respectively. The dam volume V_D computed as the product of A_D and $H_{D,mean}$, spans five orders of magnitude (12 000 m³ to
148 135×10^6 m³). The median dam volume is approximately 1.0×10^6 m³. The cumulative distributions of these dam
149 dimensions can all be fitted by lognormal distributions with very high correlation coefficients ($r^2 > 0.95$ except for W_D)
150 (Table 1).



151 4 Semi-empirical relationships

152 We created semi-empirical relationships for the 54 RSF dams in southwestern Norway that were not influenced by glaciers.
153 First, we linked the maximum dam height $H_{D,max}$ (in m) to the dam volume V_D (in 10^6 m³) (Fig. 5) by fitting a power-law
154 function (Eq. (2)):

$$155 H_{D,max} = 24.5 \cdot V_D^{1/3} \quad (2)$$

156 The exponent of $1/3$ is given by dimensional analysis, whereas the scale factor of 24.5 was fitted with a high correlation
157 coefficient r^2 of 0.73. The ratio ρ between the measured and predicted maximum dam heights ranges from 0.46 to 1.94, and
158 its cumulative frequency distribution can be fitted by a lognormal distribution. The 95th percentile of this distribution
159 ($\rho_{95} = 1.81$) yields the upper bound of the 90% prediction interval of Eq. (2). This implies that approximately 5% of RSF
160 dams in southwestern Norway have a maximum height exceeding the predicted value by 81% or more.

161 Similar power-law functions can be derived from datasets from other studies (Ermini and Casagli, 2003; Hermanns et al.,
162 2011a; Tacconi Stefanelli et al., 2015), with different scale factors, however (Table 2). The scale factor of landslide dams in
163 the Andes (Hermanns et al., 2011a) is much lower than those from other studies (10.1 vs. 21.5 to 24.5). Compared to our
164 inventory, other databases have a larger spread of the data indicated by higher ρ_{95} -values (Table 2).

165 Power-law functions are commonly used in landslide studies to relate the landslide volume to landslide frequency (e.g.
166 Dussauge et al., 2003; Guzzetti et al., 2003), but also other landslide characteristics, such as landslide area (e.g. Hovius,
167 1997). Similarly, the relationship between landslide volume and Fahrböschung, i.e. the ratio between the landslide fall height
168 and travel distance, can be fitted by power-law functions (e.g. Scheidegger, 1973; Nicoletti and Sorriso-Valvo, 1991;
169 Erismann and Abele, 2001; De Blasio, 2011). Furthermore, Oppikofer et al. (2019) found a power-law function linking the
170 run-up height of landslide-generated displacement waves to the landslide volume and distance from impact.

171 Regarding the influence of the morphologic dam classification on the dam height (Table 2), dams classified as asymmetrical
172 with thickest deposits in the distal part (Type ii in across-valley profile) are higher than dams with symmetrical deposits in
173 a symmetrical valley (Type i), but smaller than those partially blocking a valley (Type iv). In along-valley profiles, Type 2
174 dams with high thickness and steep slope are higher than Type 1 dams with low thickness and gentle slopes. Too few data
175 are available for the other dam types in along- or across-valley profiles and in plan view.

176 In narrow valleys the RSF deposits are more confined leading to thicker deposits and thus to a higher dam compared to wide
177 valleys where the deposits are unconfined and spread out over a larger surface. We calculated therefore ratio V_D (in 10^6 m³)
178 over valley width W_V (in m) and fitted following power-law with the exponent given by dimensional analysis (Fig. 6, Eq.
179 (3)):

$$180 H_{D,max} = 374 \cdot \left(\frac{V_D}{W_V}\right)^{0.5} \quad (3)$$

181 Ratio ρ between the measured and predicted maximum dam heights ranges from 0.52 to 2.36. The 95th percentile of the
182 lognormal distribution fitted to the cumulative frequency distribution of ρ equals 1.76 (ρ_{95}). This value is slightly smaller
183 than for Eq. (2) ($\rho_{95} = 1.81$). Amongst the other landslide dam inventories, only Tacconi Stefanelli et al. (2015) state W_V .
184 Fitting that dataset with Eq. (3) yields a lower scale factor of 285 and a much higher spread in values testified by lower r^2
185 and higher ρ_{95} -values (Fig. 6, Table 2).

186 Equation (3) has the expected behaviour with an increase in $H_{D,max}$ for higher volumes and a decrease for wider valleys. The
187 lateral spreading of the landslide deposits in the valley is, however, not accounted for. This could be achieved by including
188 the dam width W_D as additional parameter in a semi-empirical relationship. However, W_D is not independent from V_D and is
189 not easily predictable when using the semi-empirical equations to forecast the dam height for future landslides, except if the
190 run-out area is known. In that case, the dam area A_D (in km²) can be assessed, and the average dam height $H_{D,mean}$ (in m) can
191 be computed as the ratio V_D/A_D as an alternative proxy. For the RSF dams in southwestern Norway, $H_{D,max}$ (in m) increases
192 linearly with $H_{D,mean}$ (Fig. 7, Eq. (4)):



193 $H_{D,max} = 1.75 \cdot H_{D,mean} = 1.75 \cdot V_D/A_D$ (4)
194 The ratio ρ ranges from 0.57 to 1.72 with a value of ρ_{95} of 1.48 (lognormal distribution). This implies that approximately 5%
195 of landslide dams in southwestern Norway have a maximum height exceeding the predicted value by 48% or more. Both the
196 range of ρ and its 95th percentile are significantly smaller than for the other semi-empirical relationships. Again, only the
197 database by Tacconi Stefanelli et al. (2015) contains A_D for few dams. However, we calculated A_D from the published dam
198 width W_D and dam length L_D assuming an elliptic shape of the landslide dam. Using those calculated dam areas in Eq. (4)
199 provides a scale factor of 1.35 (Fig. 7, Table 2). Lower r^2 and higher ρ_{95} -values (0.65 and 1.84, respectively) indicate again
200 a larger spread of the data compared to the inventory of RSF dams in southwestern Norway.

201 5 Dam stability



202 Ermini and Casagli (2003) created the DBI as proxy to assess the stability of landslide dams (Eq. (5)):

$$203 DBI = \log_{10} \left(\frac{A_C}{V_D/H_{D,max}} \right) \quad (5)$$

204 With the upstream catchment area A_C in km², the dam volume V_D in 10⁶ m³ and the maximum dam height $H_{D,max}$ in m. Ermini
205 and Casagli (2003) found a lower DBI-limit (DBI_{lower}) of 2.75 below which most landslide dams in their inventory are stable,
206 and an upper DBI-limit (DBI_{upper}) of 3.08 above which most dams are unstable. A similar assessment of RSF dams in
207 southwestern Norway (Fig. 8a) leads to following observations: (a) one dam with a DBI of 2.33 has failed, but there is also
208 an eroded dam with a DBI of 2.17; (b) there are several stable dams with a DBI > 3.95, yet most dams with a DBI > 3.38
209 have failed or were eroded; (c) the proportion of unstable dams increases with the DBI (Fig. 8b) with however a significant
210 drop for high DBI-values in our inventory. Other inventories (Ermini and Casagli, 2003; Hermanns et al., 2011a; Tacconi
211 Stefanelli et al., 2015) show the same tendency with similar proportions of unstable dams for similar bins of DBI-values.
212 Landslide dams in the Andes (Hermanns et al., 2011a) have, however, higher proportions of unstable dams for given DBI-
213 values compared to landslide dams in other regions (Fig. 8b). We have therefore not considered the Andean inventory in the
214 joint analysis of dam stability for which we combined the different inventories and divided the dataset again in bins of DBI-
215 values containing 20 dams each (Fig. 8c). This histogram can be fitted by a linear regression to obtain $DBI_{lower} = 1.2$ and
216 $DBI_{upper} = 5.0$ used in Eq. (1) to assess the likelihood of a dam failure p_f .

217 6 Application to predict dam height and stability

218 6.1 Prediction of maximum dam height

219 We use the semi-empirical relationships (Eq. (2), (3) and (4)) to predict the maximum dam height generated by a future rock
220 slope failure damming a valley. We thereby use following assumptions and methods:

- 221 - The dam volume V_D is equal to the slide volume V_S times a bulking factor of 1.25 (25% volume increase due to fracturing
222 of the rock mass and porosity of the deposits) (Hung and Evans, 2004). This implies that the entire volume reaches the
223 valley and forms the dam. This is obviously the worst-case scenario as shown by Ermini and Casagli (2003) with an
224 average ratio V_D/V_S of 40% for rainfall-triggered landslides and 57% for earthquake-triggered landslides. In Norway,
225 however, numerical run-out modelling for the six unstable rock slopes used for the validation of the semi-empirical
226 relationships (see Table 3) shows that in general ca. 90% of V_S reach the valley bottom to form a dam.
- 227 - The valley width W_V used in Eq. (3) is measured on a cross-section along the centre line of the run-out area and roughly
228 perpendicular to the valley axis restricted to the flat valley bottom, i.e. slope angles smaller than 10°;
- 229 - The dam area A_D used in Eq. (4) is assessed iteratively based on the run-out area, which can be assessed using simple
230 modelling tools, such as the Fahrböschung or angle of reach (Scheidegger, 1973; Corominas, 1996) implemented in the



231 software CONEFALL (Jaboyedoff and Labiouse, 2011) or the software Flow-R (Horton et al., 2013, Oppikofer et al.,
232 2016a, 2016b) (Fig. 9): (a) as first approximation of A_D we use the run-out area in the flat valley bottom to compute
233 $H_{D,max}$; (b) we then clip the run-out area to this first approximation of the dam elevation (elevation of the valley floor
234 plus $H_{D,max}$) to obtain a new approximation of A_D , which in turn is used in Eq. (4) for a new estimation of $H_{D,max}$; (c) this
235 procedure is repeated until the difference between successive estimations of $H_{D,max}$ is smaller than a threshold of 1 m.
236 The area of the impounded lake corresponds to the contour line of the estimated dam elevation (elevation of the valley floor
237 plus $H_{D,max}$) (Fig. 9a).

238 6.2 Prediction of dam stability

239 The maximum dam height $H_{D,max}$ predicted by the semi-empirical relationships can then be used to assess the dam stability
240 using the DBI (Ermini and Casagli, 2003) (Eq. (5)). The catchment area A_C upstream of the dam can be easily assessed with
241 a “flow accumulation” GIS-function provided that the DEM covers the entire upstream catchment area. The resulting DBI-
242 values are in turn used in Eq. (1) to assess the probability of failure p_f .

243 6.3 Validation of semi-empirical relationships

244 To test the semi-empirical relationships for RSF dams in southwestern Norway, we analyzed four RSF dams in northern
245 Norway as validation dataset. Those dams are presently stable or infilled (Fig. 2b). In addition, the relationships were
246 validated by comparing predicted dam heights with results from detailed numerical run-out modelling for six unstable rock
247 slopes (see Böhme et al., 2016 for an example; NGU, 2020).
248 Table 3 shows the measured or modelled dam characteristics (V_D , W_V , A_D , A_C , $H_{D,max}$) and the predicted maximum dam
249 heights $H_{D,max}$ using the semi-empirical relationships in Eq. (2), (3) and (4). This comparison shows that Eq. (4) provides the
250 best match with measured/modelled dam heights in 8/10 cases, whereof all six potential future rock slope failures. For Eq.
251 (4) the average relative error is $\pm 13\%$, which is very small considering the relatively large uncertainties on the semi-empirical
252 relationship itself with a ρ_{95} of 1.48 (see above). For Eq. (2) and (3) the average relative errors are also acceptable when
253 considering only the four existing RSF dams in northern Norway ($\pm 29\%$ and $\pm 20\%$, respectively). Regarding the six future
254 RSF dams however, the average relative errors become unacceptable ($\pm 267\%$ and $\pm 202\%$, respectively). Possible reasons for
255 this huge discrepancy are discussed below. Based on this validation dataset we consider Eq. (4) as best possible semi-
256 empirical relationship to predict the maximum dam height $H_{D,max}$.

257 7 Discussion

258 7.1 Differences between landslide dam inventories

259 The inventory of landslide dams in southwestern Norway and other inventories used in this study (Ermini and Casagli, 2003;
260 Hermanns et al., 2011a; Tacconi Stefanelli et al., 2015) contain significant differences, notably the landslide processes
261 considered, the geological settings and the volume estimations.

262 Our inventory of landslide dams in SW Norway and the Andean inventory by Hermanns et al. (2011a) focus on rock slope
263 failures (rock avalanches and rock falls) and not on other landslide processes. Conversely, the worldwide inventory of Ermini
264 and Casagli (2003) and the Italian dataset by Tacconi Stefanelli et al. (2015) contain various landslide types (rock avalanches,
265 rock falls, debris flows, translational and rotation slides etc.). Based on the published information, it is unfortunately
266 impossible to extract only dams generated by rock slope failures from those inventories. Yet, such a separation into landslide
267 types would likely improve to comparability between the different inventories and the ensuing differences related to the
268 geological settings.



269 The relationship between the maximum dam height and dam volume (Fig. 5) shows a wide spread in values, i.e. a RSF dam
270 with a volume of 1×10^6 m³ can lead to a dam height ranging from 4 to 55 m. However, there is no significant difference
271 between our inventory and the datasets by Ermini and Casagli (2003) and Tacconi Stefanelli et al. (2015), which is reflected
272 in the power-law distributions fitted to the different inventories (Table 2). The Andean inventory (Hermanns et al., 2011a)
273 shows, however, significantly lower dam heights for a given volume compared to the other datasets (Fig. 5, Table 2). This
274 is related to the different geomorphic/tectonic settings of the Andean inventory with often tens of kilometer wide valleys,
275 compared to more Alpine settings used in our and other inventories.

276 Finally, the assessment of the dam volume is a crucial parameter for all semi-empirical relationships established in this study.
277 The approach chosen here follows the method by Hermanns et al. (2011a), i.e. the extrapolation of the topography prior to
278 the landslide dam formation using across-valley and along-valley profiles (Fig. 4b, c) to assess $H_{D,mean}$ and $H_{D,max}$.
279 Multiplying the $H_{D,mean}$ with the dam area A_D yields the dam volume V_D . The method used to estimate V_D is not specified
280 for the other inventories (Ermini and Casagli, 2003, Tacconi Stefanelli et al., 2015) as they are collections of several other
281 datasets. In the inventory by Tacconi Stefanelli et al. (2015) many volumes appear to be computed as the product of dam
282 width, dam length and dam height (in 11% of the cases or as the same product divided by a factor of 2 (in 35% of the cases).
283 This emphasizes the uncertainties linked to the volume estimates. A thorough reanalysis of the different landslide dam
284 inventories using a common approach would likely improve the reliability of the semi-empirical relationships proposed in
285 this study. A promising technique to assess the volume of landslide deposits is the Sloping Local Base Level technique
286 (Jaboyedoff et al., 2004, 2020) that uses a digital elevation model and the extent of the landslide deposits to compute the
287 possible pre-landslide topography. Jaboyedoff et al. (2020) review different techniques that can be useful to assess volumes
288 of landslides and their deposits.

289 **7.2 Dam stability assessment**

290 The dimensionless blockage index DBI (Ermini and Casagli, 2003) is widely accepted in the assessment of landslide dam
291 stability (e.g. Tacconi Stefanelli et al., 2016, 2018; Dufresne et al., 2018). Other geomorphic analyses were proposed (e.g.
292 Korup, 2004, Dong et al., 2009), but the extraction of the required parameters is more laborious and often even not feasible
293 for paleo dams, or the approach was only tested on a local inventory.

294 The DBI-values for landslide dams in southwestern Norway cover a similar range than those from other inventories (Fig. 8).
295 It is however surprising to have several stable landslide dams with DBI-values significantly higher than the "unstable limits"
296 defined in other studies, i.e. 3.08 in Ermini and Casagli (2003) or 3.57 in Tacconi Stefanelli et al. (2015). Our inventory
297 contains 16 landslide dams with a DBI > 3.57, whereof only 8 were eroded or breached and 8 are still intact. The proportion
298 of unstable dams in the bin with highest DBI-values is indeed significantly lower (4 unstable dams out of 10 dams) than in
299 the bin with second-highest DBI-values (9 out of 11) (Fig. 8b). Possible reasons for this difference with other inventories
300 are:

- 301 - In the creation of our inventory, we focused on existing lakes impounded by landslide deposits as identification criteria.
302 Landslide dams without remaining lake are thus not included, yet many of those dams were likely unstable. Extending
303 the inventory to all RSF dams might thus increase the overall proportion of unstable dams (23 out of 54), especially also
304 for higher DBI-values.
- 305 - Most dams in our inventory formed in prehistoric times and the stability assessment of these paleo dams is solely based
306 on geomorphologic observations. In other datasets (Ermini and Casagli, 2003, Tacconi Stefanelli et al., 2015) most
307 landslide events occurred in historic times and available historical records help distinguishing between intact, eroded and
308 breached dams.
- 309 - The RSF deposits impounding the lakes in southwestern Norway often have a large grain size (Fig. 1c, e, f). Grain size
310 analysis of RSF dams shows a median diameter of 0.6 to 0.9 m, and boulders of more than 2 m in diameter form up to



311 15% of the deposits (Jakobsen, 2016). In comparison, Casagli et al. (2003) obtained median grain sizes ranging from
312 0.0044 mm to 0.32 m for landslide dams in the Northern Apennines. The large grain size of RSF dams in southwestern
313 Norway could explain the relatively higher stability compared to (possibly) finer grained deposits in other parts of the
314 World. Deposits with larger grain size are more resistant to erosion and favour drainage through the rock avalanche
315 deposits (Casagli et al., 2003; Dunning, 2006; Weidinger, 2011) (Fig. 1c).

316 Using the proportion of unstable dams in bins of DBI-values for the combined inventory (Ermini and Casagli, 2003, Tacconi
317 Stefanelli et al., 2015 and our dataset) yields a much broader range for the transition zone between the “stable domain” and
318 “unstable domain” than in previous studies (Fig. 8). This reanalysis of the joint dataset is robust as it considers possible
319 outliers and it is less dependent on single values. One could for example argue to set the upper limit DBI_{upper} to the highest
320 DBI-value of all stable dams (4.37 instead of 5.0). This would imply that DBI_{upper} is solely depending on a single landslide
321 dam, which is not appropriate given the complexity of the phenomena and the uncertainties in the inventories. We did not
322 include the dataset by Hermanns et al. (2011a) into the combined inventory due to the significantly higher proportion of
323 unstable dams for given DBI-classes (Fig. 8a, b). A possible reason is the relatively lower dam heights in the Andes compared
324 to other datasets (see discussion above), which leads to lower DBI-values. Other causes for this difference could be the grain
325 size of deposits, climatic conditions and the age of the Andean dams, which are up to 60 ka old (Hermanns et al., 2004,
326 2011a, Costa and González Díaz, 2007)

327 It would be interesting to perform this stability assessment for different geological, geomorphological and climatic
328 environments, in order to obtain lower and upper DBI-limits for different conditions. This requires however more complete
329 inventories, as at least 100 or 150 landslide dams are required to obtain a sufficient number of bins (10 to 15 bins) containing
330 each a sufficient number of dams (≥ 10).

331 **7.3 Prediction of dam height using semi-empirical relations or numerical modelling**

332 Two of the proposed semi-empirical relationships rely only on the dam volume V_D (Eq. (2)), or on the ratio V_D over valley
333 width W_V (Eq. (3)). These equations are thus a quick tool to assess the dam height, yet comparison with numerical modelling
334 shows that these relationships overestimate the maximum dam height (Table 3). The third proposed semi-empirical
335 relationship using the ratio V_D over dam area A_D (Eq. (4)) provides a better match with numerical modelling results, requires
336 however a simple run-out analysis to assess the run-out area and estimate A_D (Fig. 9). A first assessment of the landslide run-
337 out area can be achieved by calculating the landslide run-out length L as a function of the landslide fall height H and the
338 volume-dependent angle of reach α (e.g. Scheidegger, 1973; Nicoletti and Sorriso-Valvo, 1991; Erismann and Abele, 2001;
339 De Blasio, 2011) (Fig. 4b). The angle of reach α is also used in more advanced computer programs, such as CONEFALL
340 (Jaboyedoff and Labiouse, 2011) or Flow-R (Horton et al., 2013), which require little to no calibration and can thus be
341 quickly applied to assess the run-out area. Yet, these tools do not provide the thickness of deposits and thus the dam height.
342 The third semi-empirical relationship $H_{D,max} = f(V_D/A_D)$ (Eq. (4)) yields the maximum dam height based on the landslide run-
343 out area and dam area.

344 Using detailed numerical simulations of the landslide propagation and run-out, such the DAN3D code (McDougall and
345 Hungr, 2004) or the RAMMS software suite (Christen et al., 2012), directly provide the thickness of landslide deposits and
346 allows to find the lowest elevation of the post-slide topography up to which a lake can form (see Oppikofer et al., 2016a,
347 Fig. 9). However, these simulations require many input parameters and extensive calibration in order to obtain reliable
348 results. These requirements impede their cost-efficient use in regional studies, where a large number of potential landslide
349 dams need to be assessed.

350 The proposed semi-empirical relationships are a conservative method because they assess the maximum dam height and thus
351 not the lowest elevation where dam overtopping may occur. Numerical simulations on the other hand provide the dam height
352 and elevation where overtopping would occur. This difference partly explains the discrepancy between numerically modelled



353 and empirically predicted dam heights (Table 3). Another possible reason for this discrepancy is the difference between
354 observed and modelled run-out areas. The effective run-out area of a landslide can be significantly smaller than numerically
355 simulated ones: the latter generally cover the entire area potentially affected by a landslide, while the real run-out area of a
356 landslide event may only cover parts of the total area. As the landslide volume in reality may spread over a smaller area than
357 simulated, the average and maximum dam heights obtained by numerical simulations or by Eq. (4) may be too small. Yet,
358 the possible overestimation of A_D is counterbalanced by conservative estimate of V_D being the entire landslide volume V_S
359 times a bulking factor of 1.25. More back-analyses of landslide-generated dams are required to ascertain these possible
360 differences between modelled and real run-out areas. In turn, this could lead to an improved workflow for assessing the dam
361 height and reducing uncertainties.

362 These considerations highlight the necessity to assess uncertainties on dam height and stability by using various approaches,
363 including different semi-empirical relationships, but also numerical simulations for critical areas. To assess uncertainties,
364 we calculate for example the DBI and p_f using $H_{D,max}$ for the potential RSF dams of the validation dataset (Table 3).
365 Compared to the results from numerical simulations, the DBI increases in average by 0.64 and 0.56 for Eq. (2) and (3),
366 respectively. This leads in turn to an average increase of p_f of +16% and +14%, respectively. This comparison highlights
367 that despite large uncertainties, the influence on dam stability and thus on the consequences assessment is relatively
368 moderate.

369 **8 Conclusions & perspectives**

370 The semi-empirical relations presented here provide a rapid approach for predicting the maximum dam height of dams that
371 might result from the future failure of an unstable rock slope. All relations require only limited input parameters, chiefly the
372 slide volume, the valley width and the dam area based on simple run-out assessments. These semi-empirical relationships
373 are established from an inventory of 54 RSF dams in southwestern Norway with dam volumes ranging from 12 000 m³ to
374 135×10^6 m³. Only dams generated by catastrophic rockslides or rock avalanches and without any glacial influence were
375 included in the analyses. Consequently, the semi-empirical relations presented here may be less or not applicable for other
376 landslide types (e.g. debris-flows, shallow landslides) and other volume classes. The upper bounds of the 90% prediction
377 intervals of these semi-empirical relationships range from 1.48 to 1.81, meaning that approximately 5% of the actual
378 maximum dam heights exceed the predicted value by 48% to 81% or more.

379 Validation of the semi-empirical relationships was performed using four RSF dams in northern Norway, but also results
380 from detailed numerical run-out simulations for six unstable rock slopes. The maximum dam heights predicted by the semi-
381 empirical relations are generally in good agreement with the measured/modelled dam heights from the validation dataset.
382 Best validation results are obtained for the relationship linking maximum dam height to landslide volume and dam area with
383 only a modest overestimation of the maximum dam heights (average relative error of 18%). This semi-empirical relationship
384 provides thus an appropriate tool for the first-order assessment of dams generated by rock slope failures at a local to regional
385 scale. Using limited input parameters, this relationship allows the prediction of the maximum dam height and thus the
386 upstream inundation area, but also to quickly forecast the dam stability using the dimensionless blockage index.

387 Possible improvements of these semi-empirical relationships are the inclusion of additional datasets, notably existing
388 landslide dams from other regions in Norway. Similar datasets could be collected for other mountainous regions in the
389 World, possibly leading to semi-empirical relationships with different parameters than those presented here for dams from
390 rock slope failures in southwestern Norway. Another possible major improvement consists in the addition of those dams that
391 do not possess a lake or residual lake at present. This requires however very time-intensive screening over large regions to
392 detect the landslide deposits that might have blocked a river in the past. Furthermore, the presented semi-empirical
393 relationships are only valid for rockslides and rock avalanches. Similar semi-empirical relationships can be imagined for



394 other landslide types, but more complete datasets on those landslide dams are required first. We strongly suggest using the
395 predictive tools developed here to assess landslide dam formation and stability, which should be an integral part of risk
396 assessment for future landslide events.

397 **Data availability**

398 Data used for this study are available on DataverseNO: Oppikofer, T., Hermanns, R.L., Jakobsen, V.U., Böhme, M., Nicolet,
399 P., Penna, I.: Database on landslide dams in southwestern Norway, DataverseNO, <https://doi.org/10.18710/47DXWT>, 2020.

400 **Author contribution**

401 RH and TO conceptualized and supervised the study; VJ created the landslide dam inventory; TO analysed the study data
402 with support from MB, PN, IP and RH; TO prepared the manuscript with contributions from all co-authors.

403 **Acknowledgements**

404 We are grateful to the Norwegian Water Resources and Energy Directorate for funding this project through the national
405 mapping program for unstable rock slopes in Norway.

406 **References**

- 407 Böhme, M., Oppikofer, T., Longva, O., Jaboyedoff, M., Hermanns, R.L., and Derron, M.-H.: Analyses of past and present
408 rock slope instabilities in a fjord valley: implications for hazard assessment. *Geomorphology*, 248, 464–474,
409 <https://doi.org/10.1016/j.geomorph.2015.06.045>, 2015.
- 410 Böhme, M., Bunkholt, H., Dehls, J.F., Oppikofer, T., Hermanns, R.L., Dalsegg, E., Kristensen, L., Lauknes, T.R., and
411 Eriksen, H.Ø.: Geologisk modell og fare- og risikoklassifisering av det ustabile fjellpartiet Gamanjuni 3 i Mandalen,
412 Troms. *Geol. Surv. Norw.*, Trondheim, Norway, NGU report 2016.031, 63 pp., 2016 (in Norwegian).
- 413 Casagli, N., Ermini, L., and Rosati, G.: Determining grain size distribution of the material composing landslide dams in the
414 Northern Apennines: sampling and processing methods. *Eng. Geol.*, 69, 83–97, [https://doi.org/10.1016/S0013-](https://doi.org/10.1016/S0013-415)
415 [7952\(02\)00249-1](https://doi.org/10.1016/S0013-7952(02)00249-1), 2003.
- 416 Christen, M., Bühler, Y., Bartelt, P., Leine, R., Glover, J., Schweizer, A., Graf, C., McArdell, B.W., Gerber, W., Deubelbeiss,
417 Y., Feistl, T., and Volkwein, A.: Integral hazard management using a unified software environment: numerical simulation
418 tool "RAMMS" for gravitational natural hazards, in: Proceedings of the 12th Congress INTERPRAEVENT, Grenoble,
419 France, 23-26 April 2012, 77–86, 2012.
- 420 Corominas, J.: The angle of reach as a mobility index for small and large landslides. *Can. Geotech. J.*, 33, 260–271, 1996.
- 421 Costa, C.H. and González D'Á, E.F.: Age constraints and paleoseismic implication of rock avalanches in the northern
422 Patagonian Andes, Argentina. *J. S. Am. Earth Sci.*, 24, 48–57, 2007.
- 423 Costa, J.E. and Schuster, R.L.: The formation and failure of natural dams. *Bull. Geol. Soc. Am.*, 100, 1054–1068,
424 [https://doi.org/10.1130/0016-7606\(1988\)100%3C1054:TFAFON%3E2.3.CO;2](https://doi.org/10.1130/0016-7606(1988)100%3C1054:TFAFON%3E2.3.CO;2), 1988.
- 425 Dai, F.C., Lee, C.F., Deng, J.H., and Tham, L.G.: The 1786 earthquake-triggered landslide dam and subsequent dam-break
426 flood on the Dadu River, southwestern China. *Geomorphology*, 65, 205–221,
427 <https://doi.org/10.1016/j.geomorph.2004.08.011>, 2005.
- 428 De Blasio, F.V.: Introduction to the physics of landslides. Springer Science & Business Media, 2011.



- 429 Dong, J.J., Tung, Y.H., Chen, C.C., Liao, J.J., and Pan, Y.W.: Discriminant analysis of the geomorphic characteristics and
430 stability of landslide dams. *Geomorphology*, 110, 162–171, <https://doi.org/10.1016/j.geomorph.2009.04.004>, 2009.
- 431 Dufresne, A., Ostermann, M., and Preusser, F.: River-damming, late-Quaternary rockslides in the Ötz Valley region (Tyrol,
432 Austria). *Geomorphology*, 310, 153–167, 2018.
- 433 Dunning, S.A.: The grain size distribution of rock-avalanche deposits in valley confined settings. *Italian Journal of*
434 *Engineering Geology and Environment*, Special issue 1, 117–121, <https://doi.org/10.4408/IJEGE.2006-01.S-15>, 2006.
- 435 Dussauge, C., Grasso, J.-R., and Helmstetter, A.: Statistical analysis of rockfall volume distributions: Implications for
436 rockfall dynamics. *J. Geophys. Res. (Solid Earth)*, 108(B6), 2286, <https://doi.org/10.1029/2001JB000650>, 2003
- 437 Erismann, T.H. and Abele, G.: *Dynamics of rockslides and rockfalls*. Springer, Berlin, 2001.
- 438 Ermini, L. and Casagli, N.: Prediction of the behaviour of landslide dams using a geomorphological dimensionless index.
439 *Earth Surf. Proc. Land*. 28, 31–47, 2003.
- 440 Etzelmüller, B., Romstad, B., and Fjellanger, J.: Automatic regional classification of topography in Norway. *Norw. J. Geol.*
441 87, 167–180, 2007.
- 442 Evans, S.G.: The formation and failure of landslide dams: an approach to risk assessment. *Italian Journal of Engineering*
443 *Geology and Environment*, Special issue 1, 15–20, <https://doi.org/10.4408/IJEGE.2006-01.S-02>, 2006.
- 444 Evans, S.G., Delaney, K.B., Hermanns, R.L., Strom, A., and Scarascia-Mugnozza, G.: The formation and behaviour of
445 natural and artificial rockslide dams; implications for engineering performance and hazard management, in: *Natural and*
446 *Artificial Rockslide Dams*, edited by: Evans, S.G., Hermanns, R.L., Strom, A., Scarascia-Mugnozza, G., *Lecture Notes in*
447 *Earth Sciences*, vol. 133, Springer, Berlin, Heidelberg, Germany, pp 1–75, 2011.
- 448 Furseth, A.: *Skredulykker i Norge*. Tun Forlag, Oslo, Norway, 2006 (in Norwegian).
- 449 Gabrielsen, R.H., Braathen, A., Dehls, J., and Roberts, D.: Tectonic lineaments of Norway. *Norw. J. Geol.*, 82, 153–174,
450 2002.
- 451 Groeber, P.: Informe sobre las causas que han producido las crecientes del río Colorado (Territorios del Neuquén y La
452 Pampa) en 1914. Ministerio de Agricultura de la Nación (Argentina), Dirección General de Minas, Buenos Aires. *Geología*
453 *e Hidrogeología, Serie B (Geología)*, Bull 11, 1–29, 1916.
- 454 Guzzetti, F., Reichenbach, P., and Wieczorek, G.F.: Rockfall hazard and risk assessment in the Yosemite Valley, California,
455 USA. *Nat. Haz. Earth Syst. Sci.*, 3, 491–503, 2003.
- 456 Hermanns, R.L., Niedermann, S., Ivy-Ochs, S., and Kubik, P.: Rock avalanching into a landslide-dammed lake causing
457 multiple dam failure in Las Conchas valley (NW Argentina) – evidence from surface exposure dating and stratigraphic
458 analyses. *Landslides*, 1, 113–122, 2004.
- 459 Hermanns, R.L., Folguera, A., Penna, I., Fauqué, L., and Niedermann, S.: Landslide Dams in the Central Andes of Argentina
460 (Northern Patagonia and the Argentine Northwest), in: *Natural and Artificial Rockslide Dams*, edited by: Evans, S.G.,
461 Hermanns, R.L., Strom, A., Scarascia-Mugnozza, G., *Lecture Notes in Earth Sciences*, vol. 133, Springer, Berlin,
462 Heidelberg, Germany, pp 147–176, 2011a.
- 463 Hermanns, R.L., Hewitt, K., Strom, A., Evans, S.G., Dunning, S.A., Scarascia-Mugnozza, G.: The Classification of
464 Rockslide Dams, in: *Natural and Artificial Rockslide Dams*, edited by: Evans, S.G., Hermanns, R.L., Strom, A., Scarascia-
465 Mugnozza, G., *Lecture Notes in Earth Sciences*, vol. 133, Springer, Berlin, Heidelberg, Germany, pp 581–593, 2011b.
- 466 Hermanns, R.L., Oppikofer, T., Anda, E., Blikra, L.H., Böhme, M., Bunkholt, H., Crosta, G.B., Dahle, H., Devoli, G.,
467 Fischer, L., Jaboyedoff, M., Loew, S., Sætre, S., and Yugi Molina, F.X.: Recommended hazard and risk classification
468 system for large unstable rock slopes in Norway, *Geol. Surv. Norw., Trondheim, Norway, NGU report 2012.029*, 52 pp.,
469 2012.
- 470 Hermanns, R.L., Blikra, L.H., Anda, E., Saintot, A., Dahle, H., Oppikofer, T., Fischer, L., Bunkholt, H., Böhme, M., Dehls,
471 J.F., Lauknes, T.R., Redfield, T.F., Osmundsen, P.T., and Eiken, T.: Systematic Mapping of Large Unstable Rock Slopes in



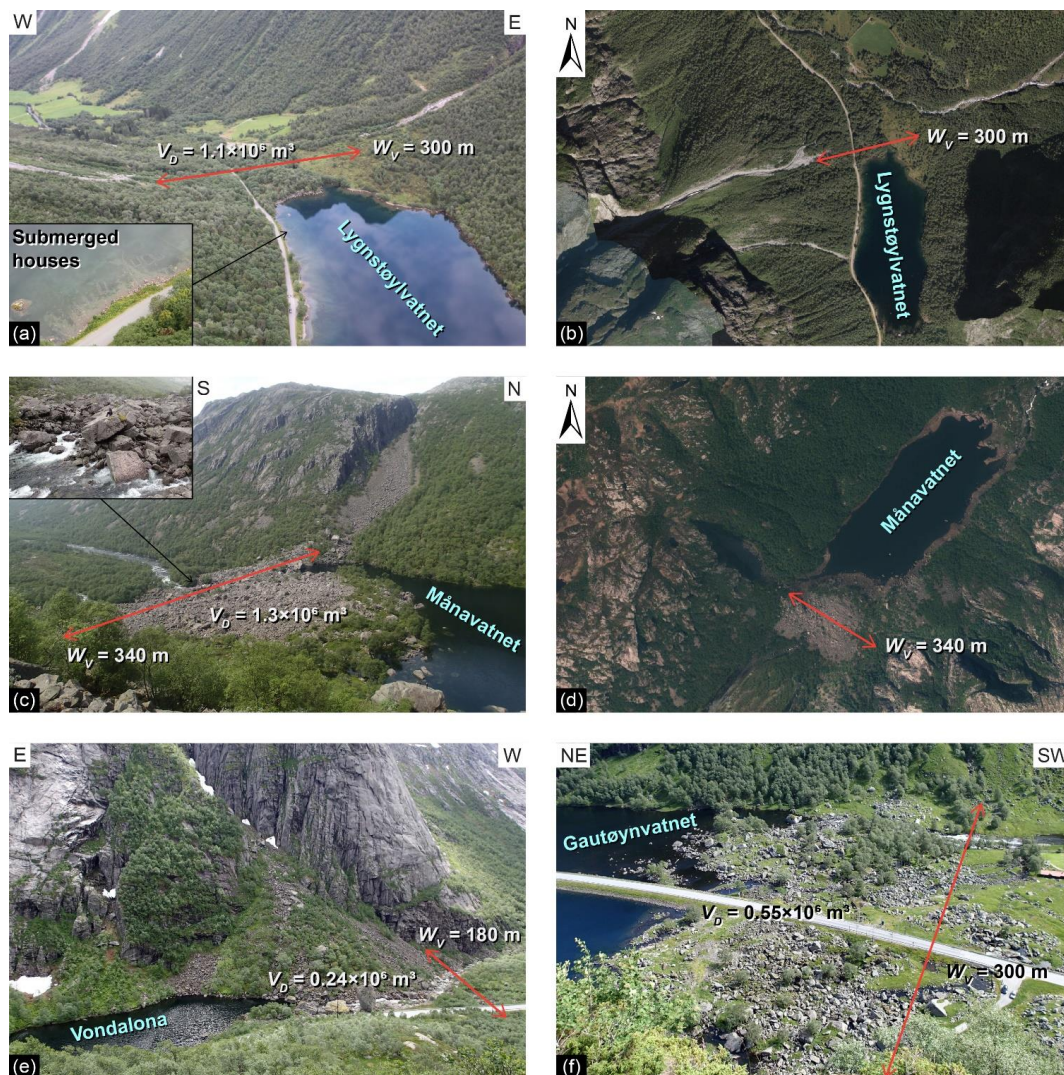
- 472 Norway, in: *Landslide Science and Practice*, vol. 1, edited by: Margottini, C., Canuti, P., and Sassa, K., Springer, Berlin,
473 Heidelberg, Germany, 29–34, 2013a.
- 474 Hermanns, R.L., Dahle, H., Bjerke, P.L., Crosta, G.B., Anda, E., Blikra, L.H., Saintot, A., and Longva, O.: Rockslide Dams
475 in Møre og Romsdal County, Norway, in: *Landslide Science and Practice*, vol. 6, edited by: Margottini, C., Canuti, P., and
476 Sassa, K., Springer, Berlin, Heidelberg, Germany, 3–12, 2013b.
- 477 Hermanns, R.L., Schleier, M., Böhme, M., Blikra, L.H., Gosse, J.C., Ivy-Ochs, S., Hilger, P.: Rock-Avalanche Activity in
478 W and S Norway Peaks After the Retreat of the Scandinavian Ice Sheet, in: *WLF 2017: Advancing Culture of Living with*
479 *Landslides*, edited by: Mikoš, M., Vilímek, V., Yin, Y., Sassa, K., Springer, Cham, Switzerland, 331–338, 2017.
- 480 Hewitt, K.: Natural Dams and Outburst Floods in the Karakoram Himalaya, in: *Hydrological Aspects of Alpine and High*
481 *Mountain Areas (Proceedings of the Exeter Symposium, July 1982)*, vol 138, International Association of Hydrological
482 Sciences, Wallingford, UK, 259–269, 1982.
- 483 Hewitt, K.: Catastrophic landslides and their effects on the Upper Indus streams, Karakoram Himalaya, northern Pakistan.
484 *Geomorphology*, 26, 47–80, 1998.
- 485 Horton, P., Jaboyedoff, M., Rudaz, B., Zimmermann, M.: Flow-R, a model for susceptibility mapping of debris flows and
486 other gravitational hazards at a regional scale. *Nat. Haz. Earth Syst. Sci.*, 13, 869–885, [https://doi.org/10.5194/nhess-13-](https://doi.org/10.5194/nhess-13-869-2013)
487 869-2013, 2013.
- 488 Hovius, N.: Sediment flux from a mountain belt derived by landslide mapping. *Geology*, 25, 231–234, 1997.
- 489 Hungr, O.: Prospects for Prediction of Landslide Dam Geometry Using Empirical and Dynamic Models, in: *Natural and*
490 *Artificial Rockslide Dams*, edited by: Evans, S.G., Hermanns, R.L., Strom, A., Scarascia-Mugnozza, G., *Lecture Notes in*
491 *Earth Sciences*, vol. 133, Springer, Berlin, Heidelberg, Germany, 463–477, 2011.
- 492 Hungr, O and Evans, S.G.: Entrainment of debris in rock avalanches: An analysis of a long run-out mechanism. *Geol. Soc.*
493 *Am. Bull.*, 116, 1240–1252, <https://doi.org/10.1130/B25362.1>, 2004.
- 494 Jaboyedoff, M. and Labiouse, V.: Technical Note: Preliminary estimation of rockfall runout zones. *Nat. Haz. Earth Syst.*
495 *Sci.*, 11, 819–828, <https://doi.org/10.5194/nhess-11-819-2011>, 2011.
- 496 Jaboyedoff, M., Baillifard, F., Couture, R., Locat, J., and Locat, P.: Toward preliminary hazard assessment using DEM
497 topographic analysis and simple mechanical modeling by means of sloping local base level, in: *Landslides: Evaluation and*
498 *Stabilization*, edited by: Lacerda, W.A., Ehrlich, M., Fontoura, A.B., and Sayão, A., Taylor & Francis Group, London, 199–
499 205, 2004.
- 500 Jaboyedoff, M., Carrea, D., Derron, M.-H., Oppikofer, T., Penna, I.M., and Rudaz, B.: A review of methods used to estimate
501 initial landslide failure surface depths and volumes. *Eng. Geol.*, in press, <https://doi.org/10.1016/j.enggeo.2020.105478>,
502 2020.
- 503 Jakobsen, V.U.: Investigation of rockslide dams in the southwestern part of Norway. Project thesis, Norwegian University
504 of Science and Technology, Trondheim, Norway, 2015.
- 505 Jakobsen, V.U.: An empirical approach for determining the evolution and behavior of rockslide dams. MSc thesis,
506 Norwegian University of Science and Technology, Trondheim, Norway, 2016.
- 507 Korup, O.: Recent research on landslide dams; a literature review with special attention to New Zealand. *Prog. Phys. Geog.*,
508 26, 206–235, <https://doi.org/10.1191/0309133302pp333ra>, 2002.
- 509 Korup, O.: Geomorphometric characteristics of New Zealand landslide dams. *Eng. Geol.*, 73, 13–35, 2004.
- 510 McDougall, S. and Hungr, O.: A model for the analysis of rapid landslide motion across three-dimensional terrain. *Can.*
511 *Geotech. J.*, 41, 1084–1097, <https://doi.org/10.1139/T04-052>, 2004.
- 512 NGU: Unstable Rock Slopes – National Database for Unstable Rock Slopes. http://geo.ngu.no/kart/ustabilefjellparti_mobil/,
513 last access: 23 April 2020.



- 514 Nicoletti, G. and Sorriso-Valvo, M.: Geomorphic controls of the shape and mobility of rock avalanches. *Geol. Soc. Am.*
515 *Bull.*, 103, 1365–1373, 1991.
- 516 Norwegian Mapping Authority: Height DTM 10 – Map Catalogue. [https://kartkatalog.geonorge.no/metadata/dddbb667-](https://kartkatalog.geonorge.no/metadata/dddbb667-1303-4ac5-8640-7ec04c0e3918)
517 [1303-4ac5-8640-7ec04c0e3918](https://kartkatalog.geonorge.no/metadata/dddbb667-1303-4ac5-8640-7ec04c0e3918), last access: 23 April 2020, 2020a.
- 518 Norwegian Mapping Authority: Norge i bilder – Online map service for orthophotos. <https://www.norgebilder.no/>, last
519 access: 23 April 2020, 2020b.
- 520 NVE: Skredatlas. <https://atlas.nve.no/Html5Viewer/index.html?viewer=nveatlas#>, last access: 23 April 2020.
- 521 Oppikofer, T., Böhme, M., Nicolet, P., Penna, I.M., and Hermanns, R.L.: Metodikk for konsekvensanalyse av fjellskred,
522 *Geol. Surv. Norw.*, Trondheim, Norway, NGU report 2016.047, 67 pp., 2016a (in Norwegian).
- 523 Oppikofer, T., Hermanns, R.L., Sandøy, G., Böhme, M., Jaboyedoff, M., Horton, P., Roberts, N.J., and Fuchs, H.:
524 Quantification of casualties from potential rock-slope failures in Norway, in: *Landslides and Engineered Slopes. Experience,*
525 *Theory and Practice*, edited by: Aversa, S., Cascini, L., Picarelli, L., and Scavia, C., Associazione Geotecnica Italiana, Rome,
526 Italy, 1537–1544, 2016b.
- 527 Oppikofer, T., Hermanns, R.L., Roberts, N.J., and Böhme, M.: SPLASH: semi-empirical prediction of landslide-generated
528 displacement wave run-up heights, in: *Subaqueous Mass Movements and Their Consequences: Assessing Geohazards,*
529 *Environmental Implications and Economic Significance of Subaqueous Landslides*, edited by: Lintern, D.G., Mosher, D.C.,
530 Moscardelli, L.G., Bobrowsky, P.T., Campbell, C., Chaytor, J.D., Clague, J.J., Georgiopoulou, A., Lajeunesse, P.,
531 Normandeau, A., Piper, D.J.W., Scherwath, M., Stacey, C., Turmel, D., Geological Society of London Special Publications,
532 477, 353–366, <https://doi.org/10.1144/SP477.1>, 2019.
- 533 Plaza, G., Zevallos, O., Cadier, E.: La Josefina Landslide Dam and Its Catastrophic Breaching in the Andean Region of
534 Ecuador, in: *Natural and Artificial Rockslide Dams*, edited by: Evans, S.G., Hermanns, R.L., Strom, A., Scarascia-
535 Mugnozza, G., *Lecture Notes in Earth Sciences*, vol. 133, Springer, Berlin, Heidelberg, Germany, 389–406, 2011.
- 536 Scheidegger, A.E.: On the prediction of the reach and velocity of catastrophic landslides. *Rock Mech.*, 5, 231–236, (1973).
- 537 Tacconi Stefanelli, C., Catani, F., and Casagli, N.: Geomorphological investigations on landslide dams. *Geoenviron.*
538 *Disasters*, 2, 21, <https://doi.org/10.1186/s40677-015-0030-9>, 2015.
- 539 Tacconi Stefanelli, C., Segoni, S., Casagli, N., and Catani, F.: Geomorphological analysis for landslide dams, in: *Landslides*
540 *and Engineered Slopes. Experience, Theory and Practice*, edited by: Aversa, S., Cascini, L., Picarelli, L., and Scavia, C.,
541 Associazione Geotecnica Italiana, Rome, Italy, 1883–1887, 2016.
- 542 Tacconi Stefanelli, C., Vilímek, V., Emmer, A., and Catani, F.: Morphological analysis and features of the landslide dams
543 in the Cordillera Blanca, Peru. *Landslides*, 15, 507–521, <https://doi.org/10.1007/s10346-017-0888-6>, 2018.
- 544 Weidinger, J.T.: Stability and life span of landslide dams in the Himalayas (India, Nepal) and the Qin Ling Mountains
545 (China), in: *Natural and Artificial Rockslide Dams*, edited by: Evans, S.G., Hermanns, R.L., Strom, A., Scarascia-Mugnozza,
546 G., *Lecture Notes in Earth Sciences*, vol. 133, Springer, Berlin, Heidelberg, Germany, 243–277, 2011.

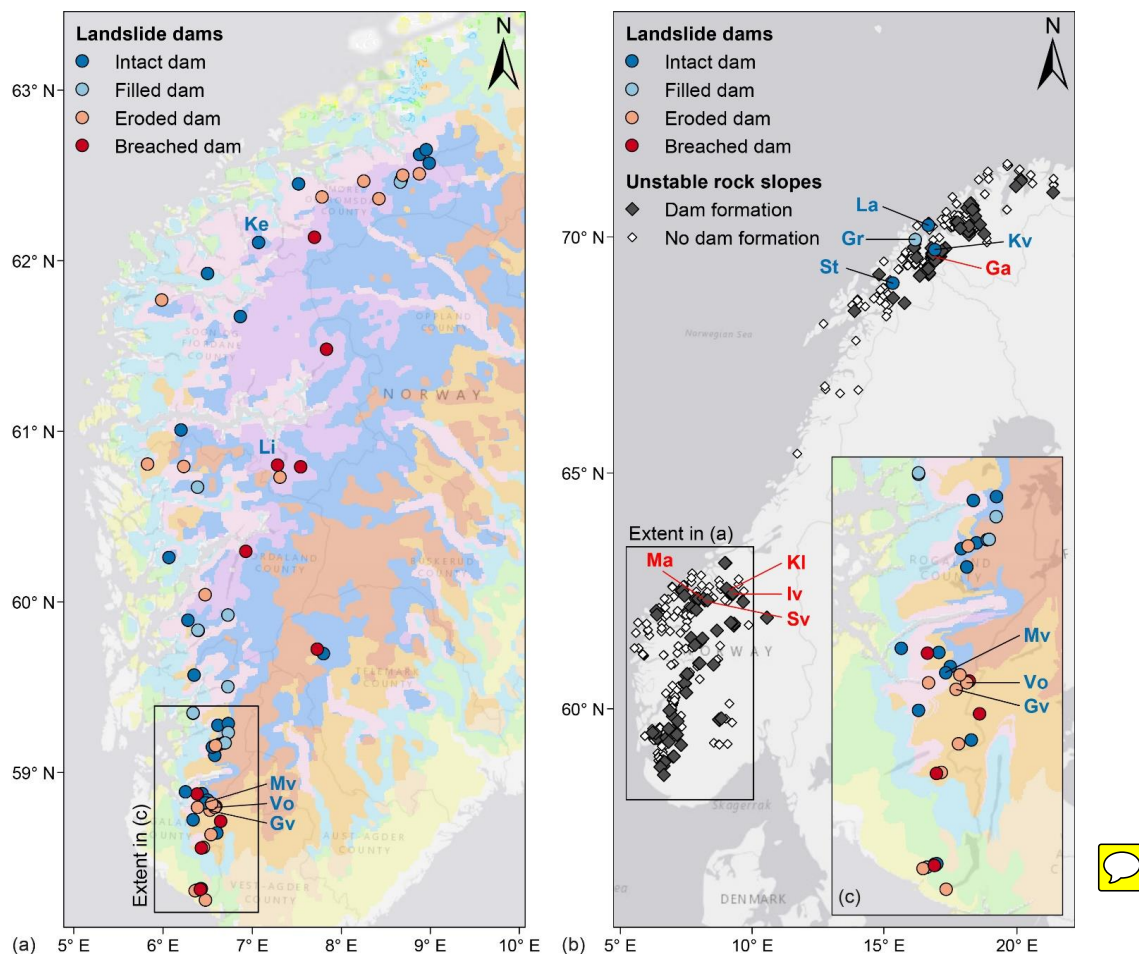


547 **Figures**



548

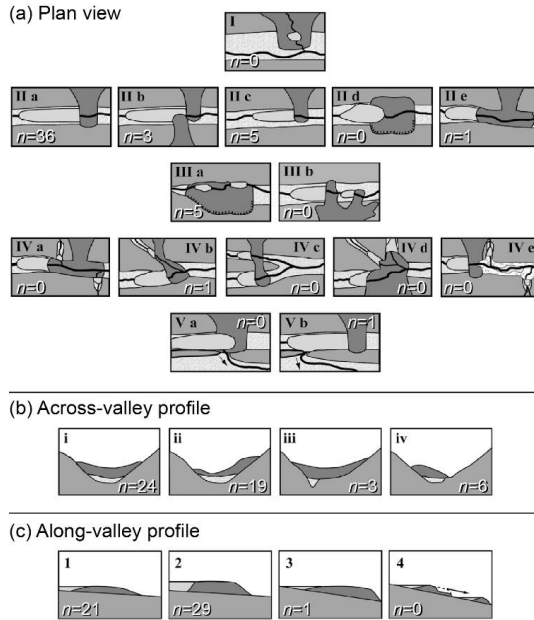
549 **Figure 1:** Photographs of RSF dams in southwestern Norway with dam volume V_D and valley width W_V : (a) the lake
550 Lygnstøylvatnet was created by the 1908 rock avalanche from the mountain Keipen in the West. The rock avalanche went over
551 an existing debris cone and abutted against a debris cone on the opposite valley side leading to a type IIb dam that is intact (dam
552 classification by Hermanns et al. 2011b). The remains of submerged houses are visible in Lygnstøylvatnet (inset); (b) orthophoto
553 of Lygnstøylvatnet (Norwegian Mapping Authority, 2020b); (c) the lake Månavatnet was dammed by a $1.3 \times 10^6 \text{ m}^3$ rock
554 avalanche coming from the Northwest. The type IIa dam is stable until now with drainage through the rock avalanche deposits
555 (inset); (d) orthophoto of Månavatnet (Norwegian Mapping Authority, 2020b); (e) the lake Vondalona was created by a small rock
556 avalanche in the narrow valley and the type IIc dam is partly eroded by the river; (f) the lake Gautøyvatnet is located only 3.7 km
557 downstream of lake Vondalona and was dammed by a $0.55 \times 10^6 \text{ m}^3$ rock avalanche that completely crossed the valley. The type
558 IIa dam is partly eroded by the river.



Landform classification (Etzelmüller et al., 2007)

□ Coastal plains and strandflat	■ Lower mountain plateaux	■ High paleic mountains with glacial incisions
■ Hills, low relief	■ Higher mountain plateaux	■ Alpine relief, mainly coastal mountains
■ Hills, accentuated relief	■ Glacially scoured low mountains and valleys	■ Extreme Alpine relief, steep slopes, heavily over-deepened valleys
■ Elevated hills/table lands, low relief		

559
 560 **Figure 2: Inventory maps of dams from rock slope failures and unstable rock slopes in Norway: (a) dam inventory of southwestern**
 561 **Norway classified according to dam stability (modified from Jakobsen, 2015) underlain by the landform classification by**
 562 **Etzelmüller et al. (2007); (b) overview map of unstable rock slopes in Norway (per December 2019) that may lead to a rockslide**
 563 **dam in case of catastrophic failure (data from NGU, 2020), along with the location of existing dams in northern Norway used as**
 564 **validation dataset; (c) zoom on the rockslide dam clusters in Rogaland County. Rock avalanche dams discussed in the text are (in**
 565 **blue font): Ke = Keipen, Li = Lintuvatnet, Mv = Mánavatnet, Vo = Vondalona, Gv = Gautøyvatnet, La = Langfjordura, Gr =**
 566 **Grøtnesura, Kv = Kvarterda, St = Steinura. Unstable rock slopes mentioned in the text are (in red font): Ga = Gamanjunni, Iv**
 567 **=Ivasnasen, Kl = Klingråket, Ma = Mannen, Sv = Svarttinden.**



568

569

570

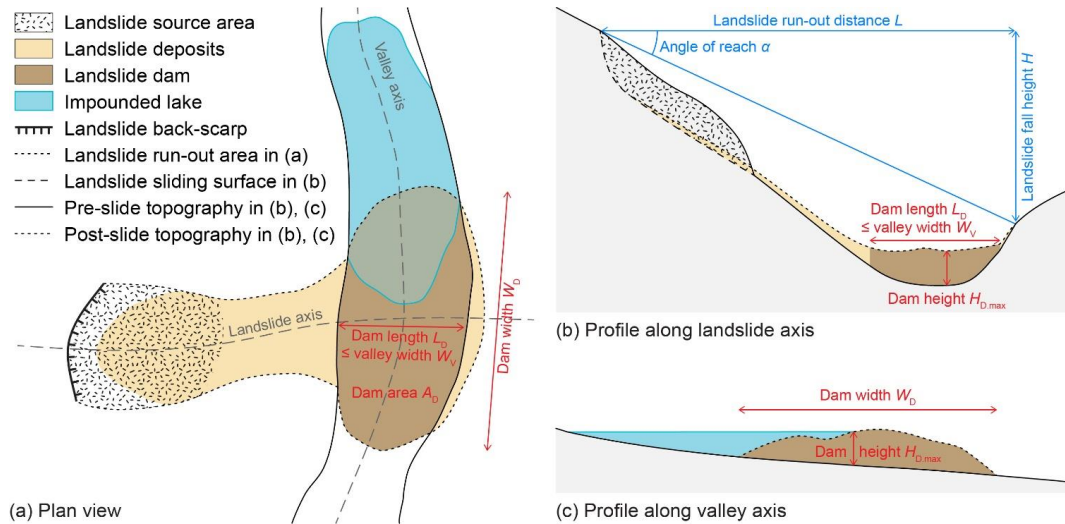
571

572

573

574

Figure 3: Morphologic classification of landslide dams (modified from Hermanns et al., 2011b) with count of landslide dams in southwestern Norway: (a) in plan view, dams formed by a landslide completely crossing the valley (Type IIa) are most common, followed by partial damming of the valley (Type IIc) and landslide dams having multiple lakes (Type IIIa); (b) in across-valley profile, most dams are symmetrical deposits in a symmetrical valley (Type i) or asymmetrical with thickest deposits in the distal part (Type ii); (c) in along-valley profile, dams with low thickness and gentle slopes (Type 1) and dams with high thickness and steep slope (Type 2) are most abundant.



575

576

577

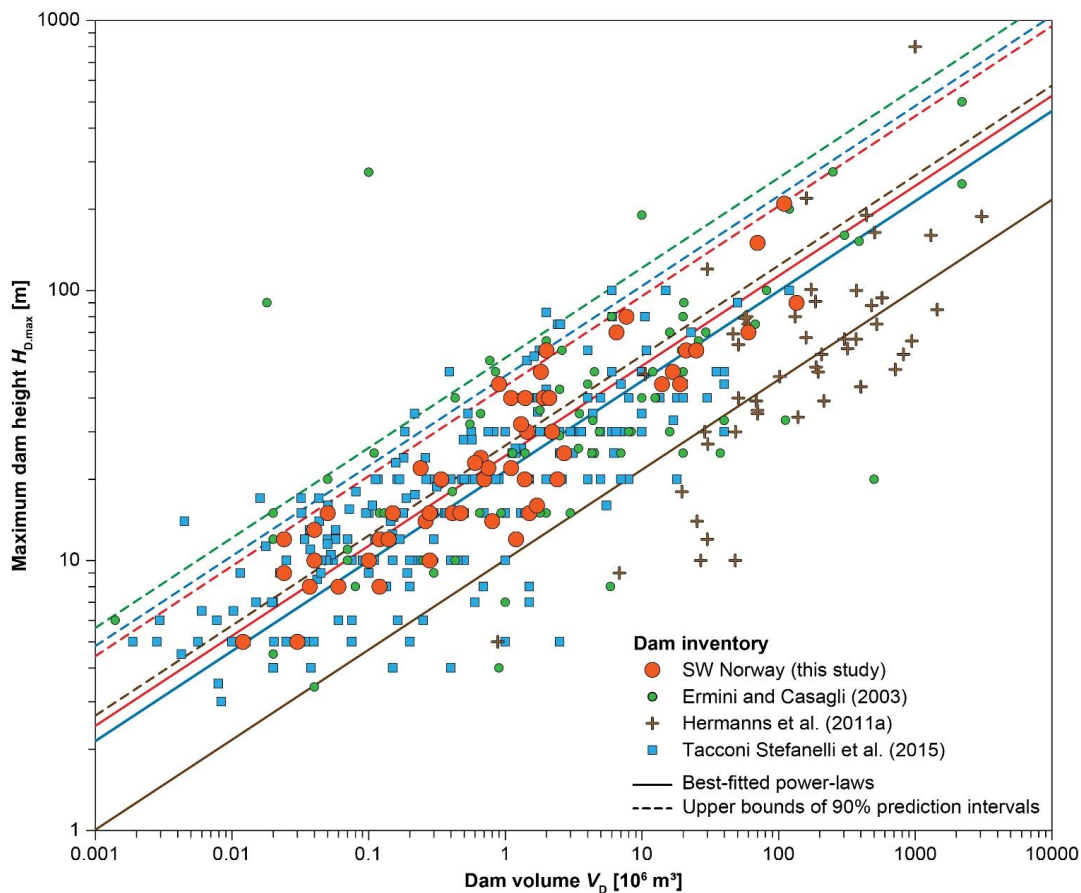
578

579

580

581

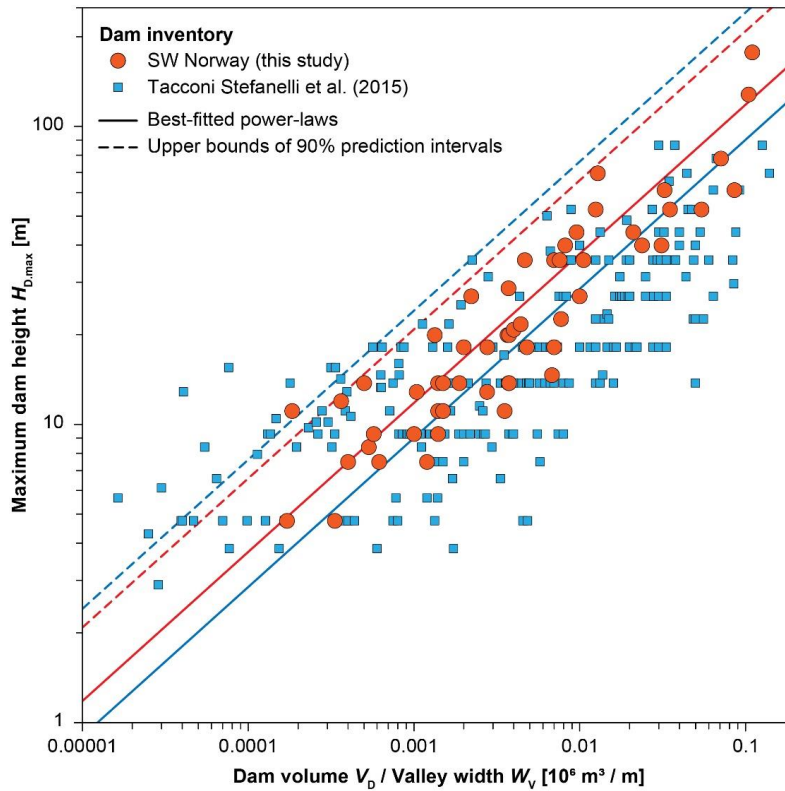
Figure 4: Sketches of a landslide dam with the measured dimensions (adapted from Toccani Stefanelli et al., 2018): (a) plan view for measuring dam area A_D , dam width W_D , dam length L_D and valley width W_V ($L_D = W_V$ in case of complete damming of valley, $L_D < W_V$ in case of partial damming of valley); (b) across-valley profile for measuring valley width W_V , dam length L_D and estimating maximum dam height $H_{D,max}$, along with landslide fall height H , landslide run-out distance L and angle of reach α ; (c) along-valley profile for measuring dam width W_D and estimating maximum dam height $H_{D,max}$. The pre-landslide topography is estimated on both profiles by considering the local valley morphology.



582

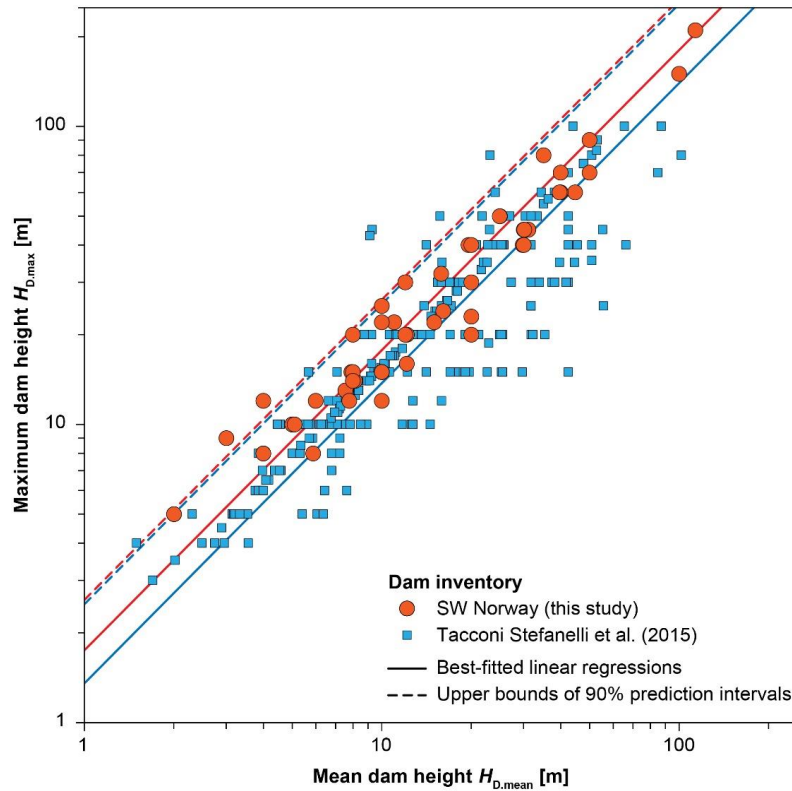
583 **Figure 5: Relationship between maximum dam height $H_{D,max}$ and dam volume V_D (in 10^6 m^3) for RSF dams in southwestern**
584 **Norway (data from Jakobsen, 2015), compared to datasets from Ermini & Casagli (2003), Hermanns et al. (2011a) and Tacconi**
585 **Stefanelli et al. (2015). The maximum dam heights increase with dam volume according to power-law distributions as in Eq. (2)**
586 **with scale factors as in Table 2 (with colours matching the point symbols).**





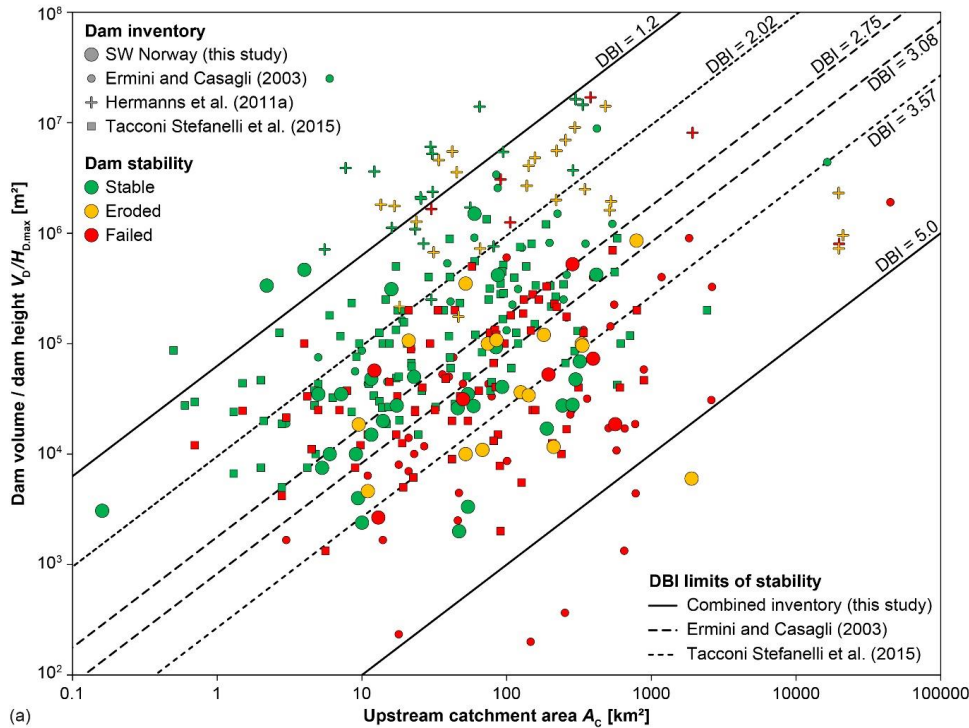
587

588 **Figure 6: Relationship between maximum dam height $H_{D,max}$ and the ratio between dam volume V_D (in 10^6 m^3) and valley width**
589 **W_V (in m) for RSF dams in southwestern Norway (data from Jakobsen, 2015), compared to the dataset from Tacconi Stefanelli et**
590 **al. (2015). $H_{D,max}$ increases with V_D/W_V according to power-law distributions as in Eq. (3) with scale factors as in Table 2 (with**
591 **colours matching the point symbols).**

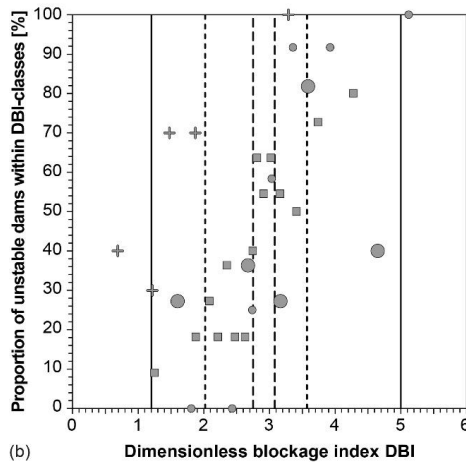


592

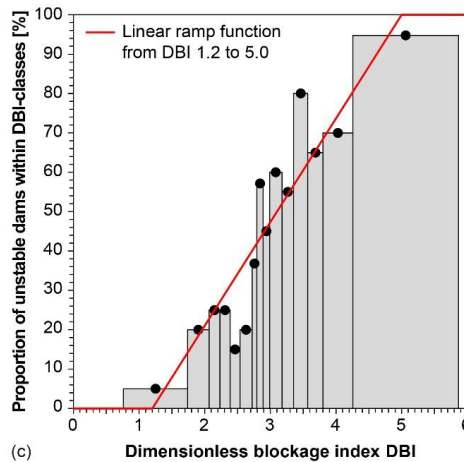
593 **Figure 7:** Linear relationship between maximum dam height $H_{D,max}$ and mean dam height $H_{D,mean}$ – computed as the ratio of dam
594 volume V_D over dam area A_D – for RSF dams in southwestern Norway (data from Jakobsen, 2015), compared to the dataset from
595 Tacconi Stefanelli et al. (2015). Linear regressions as in Eq. (4) with scale factors as in Table 2 and the upper bounds of the 90%
596 prediction intervals are shown with colours matching the point symbols.



(a)



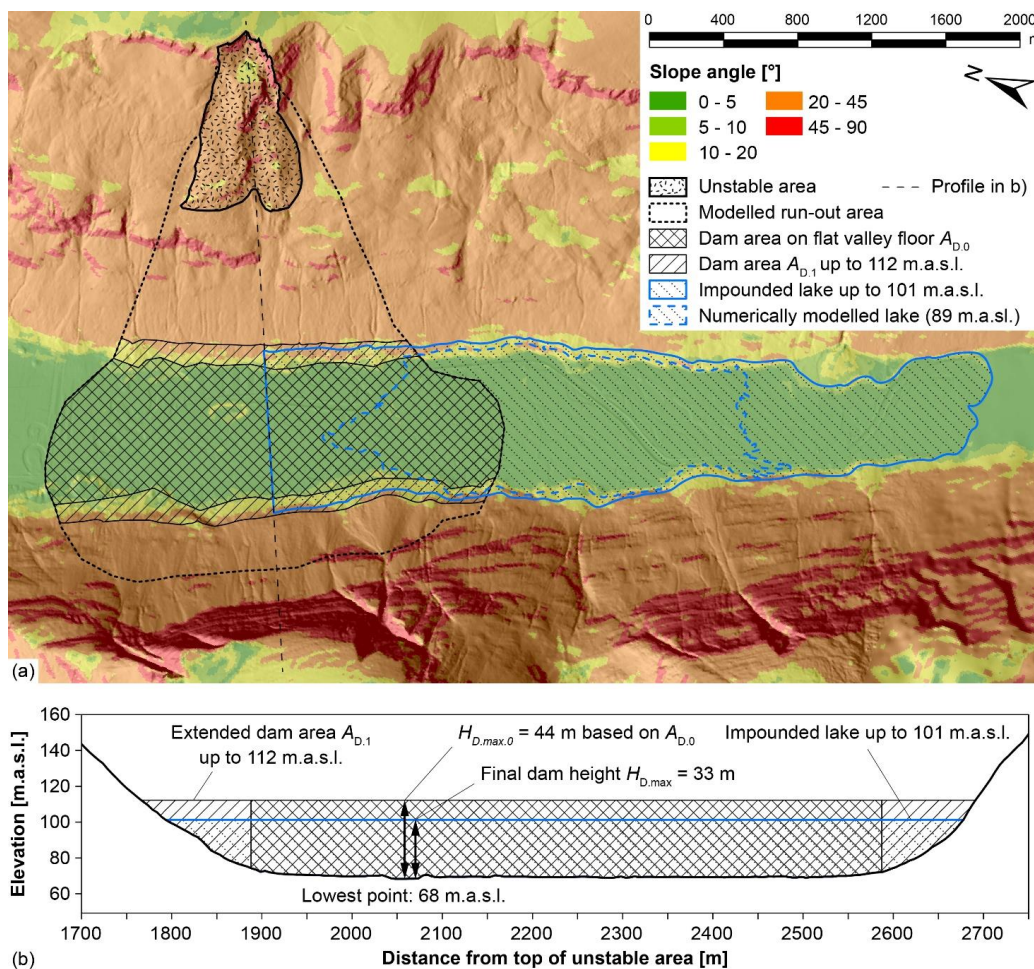
(b)



(c)

597

598 **Figure 8:** The dimensionless blockage index (DBI) for RSF dams in southwestern Norway: (a) the ratio dam volume V_D / maximum
 599 dam height $H_{D,max}$ is plotted against the upstream catchment area A_c for stable and unstable dams, along with the lower and upper
 600 DBI-limits from Ermini and Casagli (2003), Tacconi Stefanelli et al. (2015) and this study separating the stability domain from
 601 the instability domain with a transition zone in between; (b) proportions of unstable dams for bins of DBI-values (each containing
 602 10-12 landslide dams) for different inventories along with their DBI-limits (see legend in (a)); (c) for the combined inventory of
 603 landslide dams (Ermini and Casagli, 2003, Tacconi Stefanelli et al., 2015 and our dataset) the proportion of unstable dams
 604 increases with DBI. A linear function is used between DBI-values of 1.2 and 5.0 to assess the likelihood of a dam failure pr .



605

606 **Figure 9:** Iterative procedure to estimate the maximum dam height $H_{D,max}$ using the modelled run-out area to estimate the dam
 607 area A_D . The example shown is the 21×10^6 m³ rockslide of Gamanjunni 3 in Northern Norway (Böhme et al., 2016), which might
 608 lead to a 33 m high landslide dam using Eq. (4) with the iterative procedure to assess the possible dam area A_D .

609



610 **Tables**

611 **Table 1** Descriptive statistics of RSF dam dimensions in southwestern Norway and lognormal distributions matching the
 612 cumulative frequency distributions of the dimensions.

	Valley width	Dam length	Dam width	Dam area	Maximum dam height	Mean dam height	Dam volume
	W_v [m]	L_D [m]	W_D [m]	A_D [m ²]	$H_{D,max}$ [m]	$H_{D,mean}$ [m]	V_D [m ³]
Basic statistics							
Average	310	300	520	220 000	34	20	9 600 000
Median	200	200	330	53 000	21	12	1 000 000
Min	45	42	45	5000	5	2	12 000
Max	1900	1600	2800	2 700 000	210	113	135 000 000
Lognormal distribution							
Expected value (mean)	5.41	5.34	5.88	11.09	3.16	2.60	13.69
Standard deviation	0.811	0.846	0.863	1.533	0.823	0.908	2.283
r^2	0.967	0.980	0.917	0.961	0.953	0.959	0.951

613

614 **Table 2** Fitting parameters of the semi-empirical relations for different studies.

Study	Equation (2) (exponent 1/3)			Equation (3) (exponent 1/2)			Equation (4) (exponent 1)		
	Scale factor	r^2	ρ_{95}	Scale factor	r^2	ρ_{95}	Scale factor	r^2	ρ_{95}
Ermini & Casagli (2003)	21.6	0.782	2.62						
Hermanns et al. (2011a)	10.1	0.351	2.65						
Tacconi Stefanelli et al. (2015)	21.5	0.537	2.25	285	0.583	2.67	1.35	0.652	1.84
This study (all dams, $n=54$)	24.5	0.735	1.81	374	0.787	1.76	1.75	0.957	1.48
This study (Type i dams, $n=24$)	22.6	0.707	1.76	347	0.808	1.56	1.74	0.969	1.36
This study (Type ii dams, $n=19$)	27.0	0.811	1.76	395	0.838	1.77	1.65	0.977	1.45
This study (Type iv dams, $n=6$)	29.3	0.924	2.05	432	0.748	2.48	1.93	0.847	1.92
This study (Type 1 dams, $n=21$)	21.1	0.905	1.63	361	0.899	1.71	1.85	0.919	1.52
This study (Type 2 dams, $n=29$)	27.6	0.795	1.80	382	0.783	1.76	1.67	0.964	1.43

615



Table 3 Dam characteristics for past rock avalanche dams or modelled potential future rock avalanche dams in comparison with predicted dam characteristics from semi-empirical relationships. Predicted DBI-values and probability of dam failure p_f are indicated for predicted $H_{D,max}$ using Eq. (4). The predicted $H_{D,max}$, DBI- and p_f -values are shown for the best-fitted equation and in parentheses the values obtained from the upper bound of the 90% prediction interval (p_{95}). The best match between measured/modelled and empirically predicted maximum dam heights is highlighted in grey. For future landslide dams the dam volume V_D equals the landslide volume V_S times a bulking factor of 1.25 (Hungr and Evans, 2004).

Site	Dam volume V_D [10 ⁶ m ³]	Valley width W_V [m]	Dam area A_D [km ²]	Catchment area A_C [km ²]	Measured/modelled dam characteristics				Empirically predicted dam characteristics					
					Maximum dam height $H_{D,max}$ [m]	Dimension-less blockage index DBI [-]	Probability of failure p_f [%]	Maximum dam height $H_{D,max}$ [m]	Dimension-less blockage index DBI [-]	Probability of failure p_f [%]	Maximum dam height $H_{D,max}$ [m]		Dimension-less blockage index DBI [-]	
											$f(V_D)$ (Eq. (2))	$f(V_D, W_V)$ (Eq. (3))	$f(V_D, A_D)$ (Eq. (4))	DBI
Past rock avalanche dams in Northern Norway														
Grøtnesura	14.5	800	0.58	18	50	1.79	15%	60 (108)	50 (89)	44 (65)	1.73 (1.90)	14% (18%)		
Kvarteurda	16.8	620	0.44	29	60	2.02	21%	63 (114)	62 (109)	67 (99)	2.06 (2.23)	23% (27%)		
Langfjordura	15	670	0.58	5	40	1.08	0%	60 (109)	56 (99)	45 (67)	1.14 (1.31)	0% (3%)		
Steinura	12	550	0.46	21	40	1.85	17%	56 (102)	55 (97)	46 (67)	1.90 (2.07)	18% (23%)		
Potential future rock avalanche dams														
Gamanjurni	26	925	2.05	150	18	2.01	21%	73 (122)	63 (99)	22 (33)	2.11 (2.28)	24% (28%)		
Ivasnasen	2.8	220	0.31	1670	11.6	3.85	70%	34 (58)	42 (66)	16 (23)	3.98 (4.15)	73% (78%)		
Klingraket	0.29	260	0.093	2264	7.8	4.79	94%	16 (27)	12 (20)	5 (8)	4.63 (4.80)	90% (95%)		
Mannen B	24	900	2.23	1170	17	2.93	45%	70 (118)	60 (95)	18 (27)	2.96 (3.13)	46% (51%)		
Mannen C	3.6	900	0.77	1170	7	3.35	57%	38 (63)	24 (37)	8 (12)	3.43 (3.60)	59% (63%)		
Svarttinden	3.7	650	0.85	1137	6.5	3.30	55%	38 (64)	28 (44)	8 (11)	3.37 (3.54)	57% (62%)		